

Article

# Long-Term Hydropower Generation of Cascade Reservoirs under Future Climate Changes in Jinsha River in Southwest China

Yu Feng <sup>1,2</sup>, Jianzhong Zhou <sup>1,2,\*</sup>, Li Mo <sup>1,2</sup>, Zhe Yuan <sup>3</sup>, Peilun Zhang <sup>4</sup>, Jiang Wu <sup>3</sup>, Chao Wang <sup>4</sup> and Yongqiang Wang <sup>3</sup>

<sup>1</sup> School of Hydropower and Information Engineering, Huazhong University of Science and Technology, Wuhan 430074, Hubei, China; ferrychip@hust.edu.cn (Y.F.); moli@hust.edu.cn (L.M.)

<sup>2</sup> Hubei Key Laboratory of Digital Valley Science and Technology, Huazhong University of Science and Technology, Wuhan 430074, Hubei, China

<sup>3</sup> Changjiang River Scientific Research Institute, Changjiang Water Resources Commission of the Ministry of Water Resources of China, Wuhan 430010, Hubei, China; yuanzhe\_0116@126.com (Z.Y.); wujiang112@foxmail.com (J.W.); wangyq@mail.crsri.cn (Y.W.)

<sup>4</sup> China Institute of Water Resources and Hydropower research, Beijing 100038, China; peilun92@163.com (P.Z.); wangchao@iwhr.com (C.W.)

\* Correspondence: jz.zhou@hust.edu.cn; Tel.: +86-027-87543127

Received: 4 December 2017; Accepted: 15 February 2018; Published: 24 February 2018

**Abstract:** In this paper, the impact of future climate changes on long-term hydropower generation (LTHG) of cascade hydropower stations in the lower reaches of the Jinsha River is discussed. Global climate models (GCM) were used to estimate the impacts of future climate changes, the Xinanjiang model (XAJ) was applied to project the streamflow of the hydropower stations, and then gravitational search algorithm (GSA) was adopted to solve the LTHG problem. In case studies, the validation of the XAJ model shows that it perform well in the projection of streamflow in the Jinsha River. Moreover, the future hydropower generation is simulated based on five different GCMs under three climate change scenarios. Finally, the GSA algorithm is used to obtain a set of schemes under the influence of climate change. The results show that future climate changes are expected to have different impact on power generation of cascade reservoirs in the downstream of the Jinsha River when the climate change scenarios are different. These findings can provide decision support for future water resources management of the Jinsha River.

**Keywords:** long-term hydropower generation scheduling; cascade reservoirs; climate change impacts; Jinsha River

## 1. Introduction

Hydropower is a renewable energy source which plays an important role in the supply of energy. The Jinsha River is an important hydropower base in China. Four large reservoirs with 42,960 MW of total installed capacity are located downstream of the river. The main task of the four hydropower stations is to generate electricity to reduce fossil fuel consumption and environmental pollution from thermal power plants. Therefore, long-term hydropower generation scheduling (LTHG) has become an important task that must be solved. In LTHG, a major challenge is to determine the water release process of all hydropower stations at each period, and this should be done before the target time period based on hydrological forecast to satisfy the operational objectives [1]. Recent research has indicated that streamflow forecasts can have an important impact on reservoir operation. For example, Liu et al. showed that a streamflow forecast was a reliable way to select suitable reservoir inflows [2]. Xu et al. explored the use of hydrological forecast in reservoir operation [3]. Zambelli et al. proposed

annual inflow prediction for predictive control modeling [4]. Lohmann et al. presented spatio-temporal hydro-forecasts for hydro-thermal scheduling [5]. However, streamflow forecasts could be affected by various climate factors. The increase in global surface temperature in the past decades can have substantial impacts on global hydrological cycles, such as rainfall, evaporation, runoff, and soil moisture [6]. Thus, there is a need to better understand streamflow variation under climate changes and its impacts on the operation of cascade hydropower stations.

Climate change is projected to show the water resource changes in spatial and temporal distribution [7]. Under climate change scenarios, precipitation and air temperature in different river basins will be affected, and certain changes will occur in streamflow. The electricity generation of hydropower stations is strongly influenced by the total amount of streamflow, which is influenced by the regional climate pattern. Many studies have been carried out to evaluate the impact of climate change on hydropower generation. For example, Gaudard et al. have assessed climate change impacts on hydropower in the Swiss and Italian Alps [8]. Pereira et al. have implemented results from regional climate models (RCM) to study the impacts on the Iberian power system [9]. Turner et al. have combined a global hydrological and dam model to assess the impacts of climate change on hydropower and its consequences [10]. Climate change is a complex phenomenon. In the past decade, new projects have been developed to evaluate climate change, such as the fifth phase of the Climate Model Intercomparison Project (CMIP5). The CMIP5 includes new Earth system models coupled to biogeochemical components and more diagnostic output [11]. CMIP5 proposed a pack of scenarios named “Representative Concentration Pathways” (RCP) which were developed using integrated assessment models [12]. Using the dataset provided by CMIP5, we can project the change of the streamflow in the context of climate change.

The optimization of reservoir operation can increase the hydropower generation of cascade reservoirs [13] and, thus, it plays an important role in the electric power system [14]. Studies show that LTHG is a nonlinear, non-convex problem with complex constraints, including water balance, hydraulic connection, water level limits, water release limits, and output capacity limits [15–17], thus making LTHG an extremely difficult problem to be addressed. Many methods have been proposed for the optimization of reservoir operation, including dynamic programming (DP) [18,19], progressive optimality algorithm (POA) [20,21], genetic algorithm (GA) [22,23], and the gravitational search algorithm (GSA) [24,25]. Using these methods, the LTHG problem can be solved effectively.

In this paper, we evaluate the impacts of future climate changes on LTHG in the Jinsha River. Firstly, to consider the effects of future climate changes, we used the Xinanjiang (XAJ) model [26,27] coupled with global climate model (GCM) to simulate daily streamflow in the future. The XAJ model was evaluated based on the linear regression correlation coefficient and Nash-Sutcliffe efficiency coefficient [28]. Then, the total generation of the cascade hydropower stations is obtained using the GSA algorithm. Since studies have indicated that different GCMs may result in different results [29–31], the impact of future climate change is simulated based on five GCMs under three different climate change scenarios. In case studies, comparison among different algorithms shows GSA can solve LTHG problems effectively. The validation of XAJ model shows that it perform well in projection of streamflow in Jinsha River. Moreover, future climate changes are expected to have different impact on power generation of cascade reservoirs in the downstream of the Jinsha River when the climate change scenarios are different.

The rest of this paper is organized as follows: Section 2 describes the formula and constraints of LTHG operation problems; Section 3 describes the streamflow project method considering future climate changes; Section 4 describes the GSA method and implantation of the long-term scheduling model; Section 5 describes impact of future climate changes on reservoir scheduling in the Jinsha River; and Section 6 provides the summary of this paper.

## 2. The LTHG of Cascade Reservoirs

The main purpose of LTHG is to improve the power generation of cascade reservoirs [32]. The objective function is shown below.

### 2.1. Study Area

The Jinsha River is the upper reach of the Yangtze River and it flows through Qinghai, Sichuan, and Yunnan provinces in Western China. The locations of hydrological stations in the Jinsha River Basin are shown in Figure 1. The Jinsha River is rich in water resources, and it is the largest water and electricity energy base in China. A number of hydropower stations have been constructed or are currently under construction in the Jinsha River. In this paper, four cascade hydropower stations (Wudongde, Baihetan, Xiluodu, and Xiangjiaba), with a total installed capacity of 42,960 MW, are considered in this study, and their major parameters are shown in Table 1.

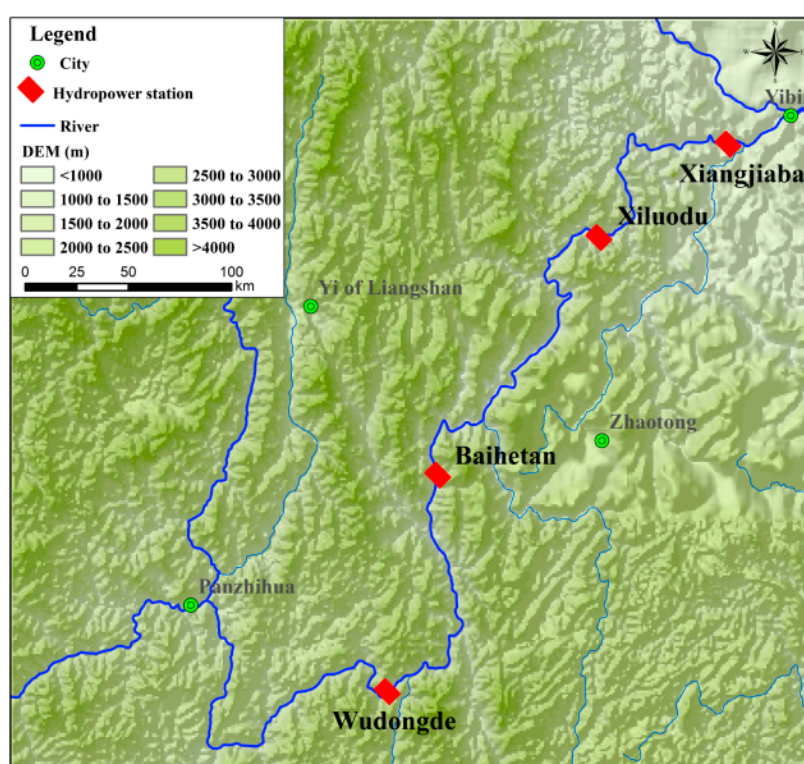


Figure 1. Locations of hydrological stations in the Jinsha River.

Table 1. Main parameters of the four cascade hydropower stations in Jinsha River.

Parameters	Wudongde	Baihetan	Xiluodu	Xiangjiaba
Dead water level (m)	945	765	540	370
Normal water level (m)	977	825	600	380
Flood limit water level (m)	952	785	560	370
Installed capacity (10 <sup>4</sup> kw)	1020	1600	1260	600
Total capacity (10 <sup>8</sup> m <sup>3</sup> )	74.08	206.27	126.7	51.63
Minimum outflow (m <sup>3</sup> /s)	906	905	1500	1500

### 2.2. The LTHG Scheduling Model

In LTHG, power generation of a single reservoir at time period *t* is determined by the generation flow and water head. As shown in Figure 1, the topology of the four reservoirs in Jinsha River is shown in Figure 2.

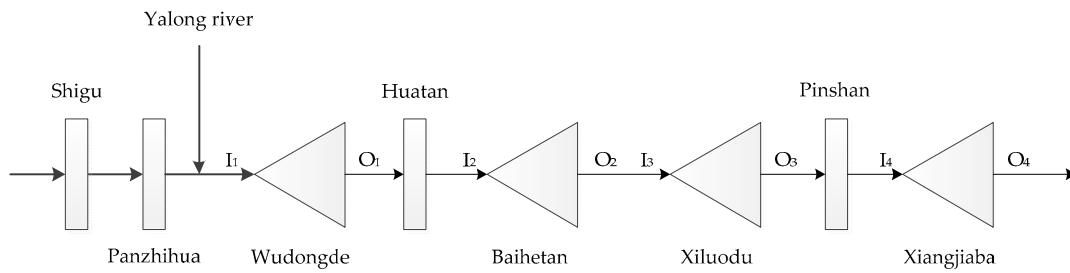


Figure 2. Topology of hydrological stations in the Jinsha River.

For a single reservoir  $i$ , the outflow consist of generation flow and spillage, and the inflow of the downstream reservoir is determined by the upstream reservoir:

$$O_{i,t} = Q_{i,t} + S_{i,t} \tag{1}$$

$$I_{i,t} = O_{i-1,t} + \Delta I_{i,t} \tag{2}$$

where  $Q_{i,t}$  is the generation flow,  $S_{i,t}$  is the spillage.  $I_{i,t}$  is the inflow of reservoir  $i$  at time  $t$ ,  $O_{i-1,t}$  is the outflow of reservoir  $i - 1$ .  $\Delta I_{i,t}$  is the interval flow between two hydropower stations.

There are four hydrological stations located on this this section of the river, including Shigu, Panzhihua, Huatan, and Pingshan. The streamflow of the four hydrological stations can be projected using the methods discussed in Section 3. However, the streamflow from Yalong River cannot be forecast because of the lack of hydrological data. The inflow of Wudongde is generalized using the streamflow of Huatan station, and the interval inflow between Baihetan and Xiluodu is generalized using the streamflow of Pingshan station:

$$I_1 = Q_{\text{Huatan}} \tag{3}$$

$$\Delta I_3 = Q_{\text{Pingshan}} - Q_{\text{Huatan}} \tag{4}$$

The generation at time  $t$  can be evaluated using the following equation:

$$E_{i,t} = k_i Q_{i,t} H_{i,t} \Delta t \tag{5}$$

where  $E_{i,t}$  is the hydropower generation of reservoir  $i$  at time period  $t$ .  $Q_{i,t}$  is the generation flow through the hydropower units of reservoir  $i$  at time  $t$ .  $k_i$  is the comprehensive benefit coefficient of reservoir  $i$ , which reflect the efficiency of hydro-generating units.  $\Delta t$  is the length of time interval.  $H_{i,t}$  is the net water head of reservoir  $i$  at time  $t$  following:

$$H_{i,t} = \frac{Z_{i,t-1} + Z_{i,t}}{2} - Z_{d_{i,t}} - \Delta H_i \tag{6}$$

where  $Z_{i,t-1}$  and  $Z_{i,t}$  are start water level and end water level of reservoir  $i$  at time  $t$ .  $Z_{d_{i,t}}$  is the water level under the dam.  $\Delta H_i$  is the water head loss of reservoir  $i$ .

Overall, the objective of the LTHG scheduling model is to find a set of water releases or storage volumes to maximize the LTHG of cascade hydropower stations, which can be described mathematically as follows:

$$E = \max \sum_{t=1}^T \sum_{i=1}^N E_{i,t} \tag{7}$$

where  $E$  is the total hydropower generation of cascade reservoirs,  $T$  is the number of periods, and  $N$  is the number of reservoirs.

### 2.3. Constraints

The following constraints are considered in this study:

- (1) Water balance constraint:

$$V_{i,t} = V_{i,t-1} + (I_{i,t} - O_{i,t}) \cdot \Delta t \quad (8)$$

where  $V_{i,t}$  is the storage of reservoir  $i$  at time  $t$ .

- (2) Water level constraint:

$$Z_{i,t}^{\min} \leq Z_{i,t} \leq Z_{i,t}^{\max} \quad (9)$$

$$|Z_{i,t} - Z_{i,t-1}| \leq Z_{i,t}^{\text{step}} \quad (10)$$

where  $Z_{i,t}^{\min}$  and  $Z_{i,t}^{\max}$  are the lower and upper bounds of the water level, respectively, and  $Z_{i,t}^{\text{step}}$  is the limit of the water level variation.

- (3) Outflow constraint:

$$O_{i,t}^{\min} \leq O_{i,t} \leq O_{i,t}^{\max} \quad (11)$$

where  $O_{i,t}^{\min}$  and  $O_{i,t}^{\max}$  are the minimum and maximum outflows of reservoir  $i$ , respectively.

- (4) Output constraint:

$$N_{i,t}^{\min} \leq N_{i,t} \leq N_{i,t}^{\max} \quad (12)$$

where  $N_{i,t}^{\min}$  and  $N_{i,t}^{\max}$  are the minimum and maximum power outputs of reservoir  $i$ , respectively.

- (5) Boundary conditions:

$$Z_{i,0} = Z_{i,\text{start}}, Z_{i,T} = Z_{i,\text{end}} \quad (13)$$

where  $Z_{i,\text{start}}$  and  $Z_{i,\text{end}}$  are the initial and terminal water levels of reservoir  $i$ , respectively.

## 3. Streamflow Forecast Considering Future Climate Impacts

In the LTHG model, the value of reservoir inflow depends on the hydrological streamflow forecast. Moreover, climate change and variability are expected to have an impact on the precipitation and runoff, which can serve as the inflow of a reservoir [33]. In this section, we discuss the streamflow project model for cascade reservoirs in the Jinsha River considering future climate impacts.

### 3.1. Observed Hydrological Data

The historical observed daily precipitation and temperature (maximum and minimum) data are collected from China's Ground Precipitation  $0.5^\circ \times 0.5^\circ$  Gridded Dataset (V2.0) and China's Ground Temperature  $0.5^\circ \times 0.5^\circ$  Gridded Dataset (V2.0) (<http://data.cma.cn/>), respectively. The dataset covers 2474 national meteorological stations over the Chinese mainland. It consists of a series of daily observed data from 1961 to the present. We use data from 208 grid boxes associate with the Jinsha River, shown in Figure 3.

Daily streamflow data was collected from hydrological stations in the lower reaches of the Jinsha River, and is used to calibrate and validate the parameters of the hydrological model. Information of the hydrological stations is shown in Table 2.

**Table 2.** Information of hydrological stations in the Jinsha River.

Station	Location (N, E)	Catchment Area ( $10^3 \text{ km}^2$ )	Data Period
Shigu	(99.96, 26.87)	269.34	1961–2000
Panzhihua	(101.72, 26.58)	281.56	1966–2000
Huatan	(102.88, 26.88)	447.78	1977–2000
Pingshan	(104.17, 28.63)	478.68	1961–2000

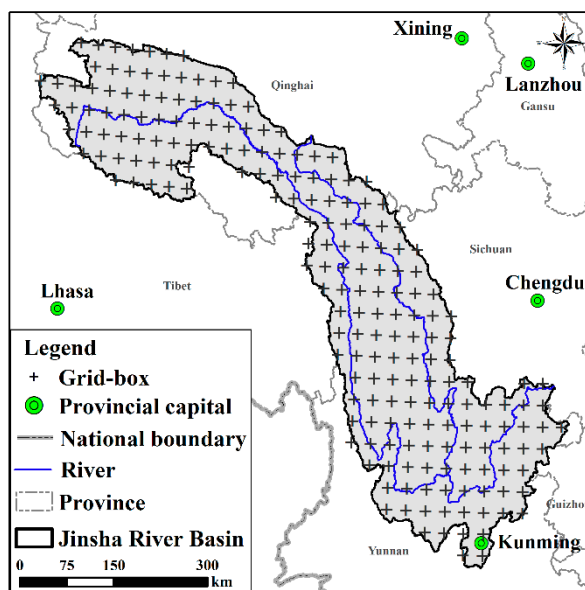


Figure 3. Grid boxes in the Jinsha River.

### 3.2. Future Climate Data

The interactions of important drivers of climate can be simulated using quantitative methods in climate models. In this study, future climate change scenarios are obtained from the Inter-Sectoral Impact Model Intercomparison Project (ISI-MIP, <http://www.isi-mip.org>). This project is designed to enable quantitative synthesis of climate change impacts at different levels of global warming [34]. Continuous daily precipitation and temperature data on a horizontal grid with  $0.5^\circ \times 0.5^\circ$  resolution for the period 1960–2099 were offered by five GCMs, including GFDL-ESM2M, HADGEM2-ES, IPSL-CM5A-LR, MIROC-ESM-CHEM, and NORESM1-M. Table 3 shows the information of the five GCMs.

Table 3. Information of selected GCMs.

Centre	Country	Name
Geophysical Fluid Dynamics Laboratory (GFDL)	United States	GFDL-ESM2M
Hadley Centre for Climate Prediction and Research, Met Office	United Kingdom	HADGEM2-ES
L’Institut Pierre-Simon Laplace (IPSL)	France	IPSL-CM5A-LR
Technology, Atmosphere and Ocean Research Institute, and National Institute for Environmental Studies	Japan	MIROC-ESM-CHEM
Norwegian Climate Centre	Norway	NORES1-M

Output of the climate model was spatially interpolated using a bilinear interpolation method, and the data has already been bias-corrected using a trend-preserving bias correction method [35]. The bias correction method modifies the monthly mean and daily variability of the simulated data to match the observations. Firstly, the long-term differences in a specific month, such as April, between simulated and observed monthly mean data are adjusted as follows:

$$\begin{cases} C = \left( \sum_{i=1}^{m=N} T_i^{WFD} - \sum_{i=1}^{m=N} T_i^{GCM} \right) / N \\ T_{ij,correct}^{GCM} = C + T_{ij}^{GCM} \end{cases} \quad (14)$$

$$\begin{cases} c = \frac{\sum_{i=1}^{m=N} P_i^{WFD}}{\sum_{i=1}^{m=N} P_i^{GCM}} \\ P_{ij,correct}^{GCM} = c \cdot P_{ij}^{GCM} \end{cases} \quad (15)$$

where  $T_i^{WFD}$  and  $P_i^{WFD}$  are monthly means of observational data for year  $i$ .  $T_i^{GCM}$  and  $P_i^{GCM}$  are monthly means of the simulated GCM data.  $N$  is the length of the reference period.  $T_{ij,correct}^{GCM}$  and  $P_{ij,correct}^{GCM}$  are corrected reference temperatures and precipitation for year  $i$  and day  $j$  in the specific month. Then, daily variability of the simulated data is corrected using a transfer function:

$$\begin{cases} \Delta T_{ij}^{GCM} = T_{ij}^{GCM} - T_i^{GCM} \\ f(\Delta T^{GCM}) = B \cdot \Delta T^{GCM} \end{cases} \quad (16)$$

$$\begin{cases} \delta P_{ij}^{GCM} = P_{ij}^{GCM} / P_i^{GCM} \\ \hat{P}_{ij}^{GCM} = \begin{cases} P_{ij}^{GCM} + m_i^{GCM} & , \text{ if wet} \\ 0 & , \text{ if dry} \end{cases} \\ \delta \hat{P}_{ij}^{GCM} = \frac{\hat{P}_{ij}^{GCM}}{\hat{P}_i^{GCM}} \\ g(\delta P^{GCM}) = [a + b \cdot \{\delta \hat{P}^{GCM} - \delta \hat{P}_{min}^{GCM}\}] \times \left[ 1 - \exp\left\{-\frac{\delta \hat{P}^{GCM} - \delta \hat{P}_{min}^{GCM}}{\tau}\right\} \right] \end{cases} \quad (17)$$

where  $B$  is the slope of a linear regression on the rank ordered WATCH Forcing Data (WFD) and GCM data.  $m_i^{GCM}$  is a constant which represents the total amount of precipitation from dry days divided by the number of wet days.  $a$  is the offset,  $b$  is the slope, and  $\tau$  is the decay constant.

In this paper, three scenarios, including RCP2.6, RCP4.5, and RCP8.5, are selected to allow for quantification of the uncertainty in the impacts of climate change at different levels of global warming.

### 3.3. XAJ Hydrological Model

The main hydrological model used for streamflow forecasting is the Xinanjiang (XAJ) model. The XAJ model is a conceptual watershed model that is widely used for runoff estimation and streamflow forecast [36,37]. Using the XAJ model, the streamflow of Huatan and Pingshan stations can be predicted.

The XAJ model is made up by four modules, including evapotranspiration calculation, runoff calculation, water division calculation, and runoff routing calculation.

The flowchart of the XAJ model is shown in Figure 4. As shown in Figure 4, the XAJ model is driven with the daily precipitation ( $P$ ) and potential evapotranspiration ( $PE$ ). In this study, the Jinsha River Basin is divided into four sub-catchments, as shown in Figure 5. The outflow of each sub-catchment is routed using the Muskingum method [38]:

$$Q_{0,t} = C_0 \times Q_{i,t-1} + C_1 \times Q_{i,t} + C_2 \times Q_{0,t-1} \quad (18)$$

$$C_0 + C_1 + C_2 = 1 \quad (19)$$

where  $C_0$ ,  $C_1$ , and  $C_2$  are the Muskingum parameters,  $Q_{i,t-1}$  and  $Q_{i,t}$  are the inflow of the reach at time  $t$  and  $t - 1$ .  $Q_{0,t-1}$  and  $Q_{0,t}$  are outflow of the reach at time  $t$  and  $t - 1$ , respectively.

The daily precipitation of each sub-catchment is evaluated following:

$$P = \frac{\sum_{i=1}^N P_i S_i}{\sum_{i=1}^N S_i} \quad (20)$$

where  $P$  is the average precipitation of the sub-catchment,  $P_i$  is the precipitation of the grid box  $i$ ,  $S_i$  is the area of grid box  $i$ .  $N$  is the number of grid boxes in the sub-catchment.

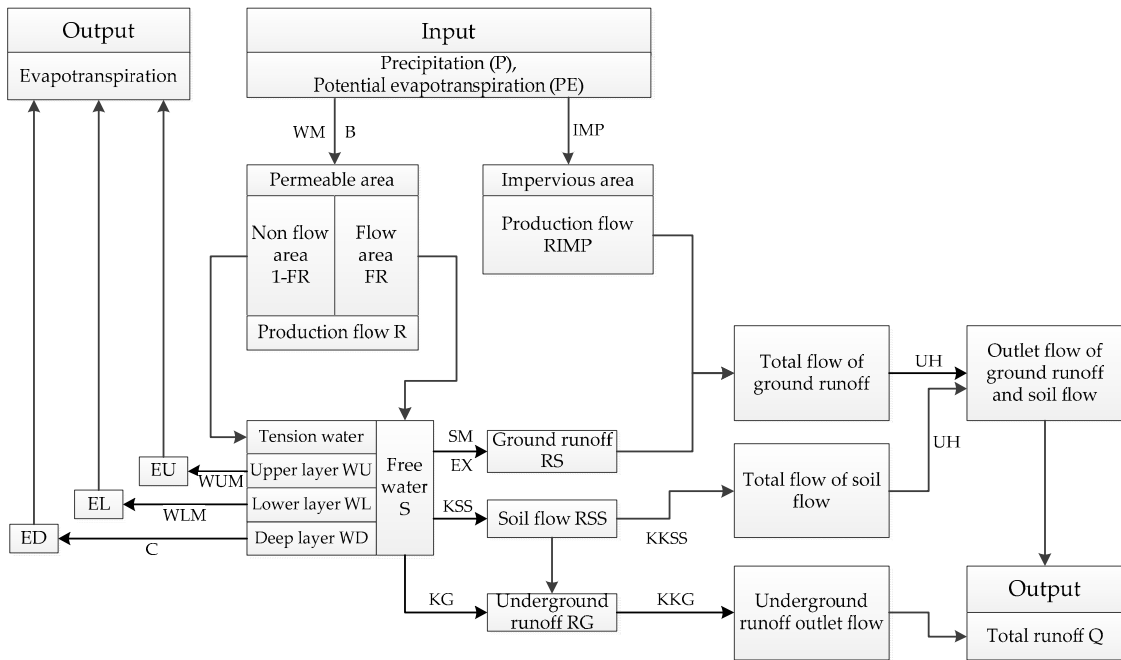


Figure 4. Flowchart of Xinanjiang model.

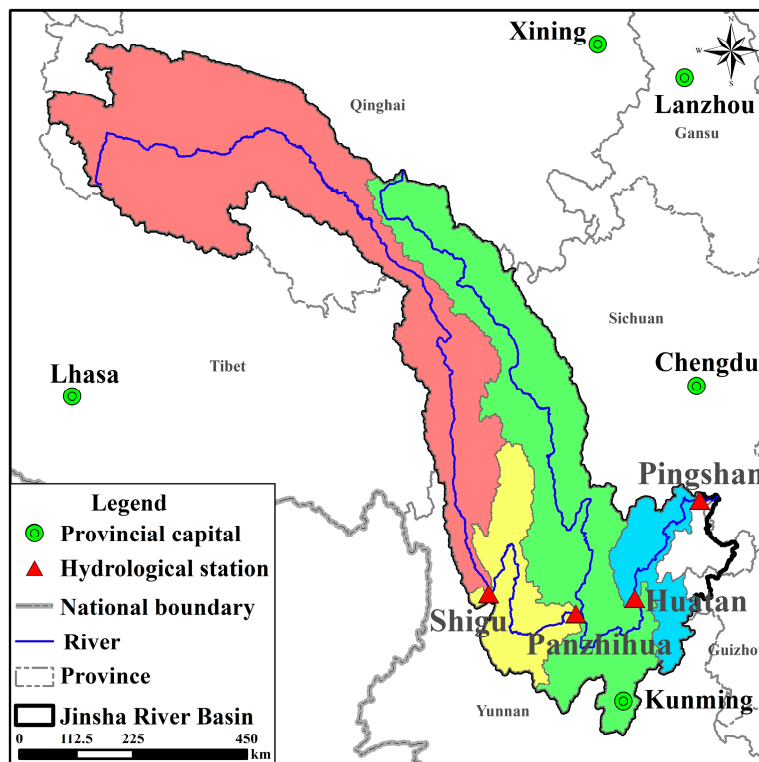


Figure 5. Sub-catchments in the Jinsha River.

The daily potential evapotranspiration of each grid is calculated using Hargreaves method [39]:

$$ET_0 = H_A \cdot R_e(T + 17.8) \cdot \Delta T^{H_E} \tag{21}$$

where  $H_A$  and  $H_E$  are the parameters with standard values of 0.0023 and 0.5, respectively.  $R_e$  is the extraterrestrial radiation.  $T$  is the mean temperature ( $T = (T_{max} + T_{min})/2$ ) and  $\Delta T$  is the air temperature range ( $\Delta T = T_{max} - T_{min}$ ). The daily evapotranspiration of each sub-catchment is calculated in the same way with precipitation.

The parameters of XAJ model shown in Table 4 is calibrated using the observed hydrological data in Section 3.1. The calibrate method is based on [40]. Performance of the XAJ model is assessed based on the linear regression correlation coefficient and the Nash-Sutcliffe efficiency coefficient [28]. The linear regression correlation coefficient can characterize the accuracy of XAJ model. The formula is as follows:

$$R = \frac{\left[ \sum_{i=1}^n (R_i^{sim} - \overline{R^{sim}}) (R_i^{obs} - \overline{R^{obs}}) \right]}{\sum_{i=1}^n (R_i^{obs} - \overline{R^{obs}})^2 \sum_{i=1}^n (R_i^{sim} - \overline{R^{sim}})^2} \tag{22}$$

where  $R$  is the linear regression correlation coefficient,  $R_{sim,i}$  is the simulated runoff at time  $i$ ,  $R_{obs,i}$  is the observed runoff at time  $i$ , and  $R_{obs}$  and  $R_{sim}$  are the observed and simulated runoff, respectively.

**Table 4.** Main parameters of the Xinanjiang model.

Parameter	Physical Meaning	Range
WUM (mm)	Soil moisture storage capacity of the upper layer	5–100
WLM (mm)	Soil moisture storage capacity of the lower layer	50–90
WDM (mm)	Soil moisture storage capacity of the deep layer	15–90
B	Exponent of surface tension storage capacity	0.1–2
IMP (%)	Percentage of impervious area	0–0.03
K	Coefficient of evaporation capacity	0.2–3.0
C	Evaporation and distribute coefficient of the deep layer	0.05–0.3
SM (mm)	Free water storage capacity	20–100
EX	Exponent of the free water capacity curve	0.1–2.0
KSS	Outflow coefficients of the free water storage to soil water	0.05–0.6
KG	Outflow coefficients of the free water storage to groundwater	0.1–0.65
KKSS	Recession constants of the soil water	0.6–0.99
KKG	Recession constants of the groundwater	0.99–0.998
UH	Recession constants of river water	0.01–0.7
KE	Parameter of the Muskingum method	0–4
XE	Parameter of the Muskingum method	0–0.5

The Nash-Sutcliffe efficiency coefficient can be expressed as follows:

$$E_{NS} = 1 - \frac{\sum_{i=1}^n (R_i^{sim} - R_i^{obs})^2}{\sum_{i=1}^n (R_i^{obs} - \overline{R^{obs}})^2} \tag{23}$$

where  $E_{NS}$  is the Nash-Sutcliffe efficiency coefficient. The forecast model performs well when  $E_{NS} \geq 0.75$ , basically well when  $0.36 < E_{NS} < 0.75$ , and poorly when  $E_{NS} \leq 0.36$ , respectively [41].

### 3.4. Correction of Forecast Results

The data provided by GCMs reflect trends of precipitation and temperature in different scenarios. However, there is a certain error in daily precipitation and temperature data provided by the GCMs and the historical observed data. When applying output from GCMs to the XAJ model, the streamflow results obtained also have errors that cannot be ignored. Therefore, the simulated results need to be corrected. In this study the Delta method was used to correct the simulated streamflow driven by the output from GCMs [42]. This method is formulated as follows:

$$x_{correct,i,j} = \frac{\overline{x_{obs,i}}}{\overline{x_{G\_His,i}}} \times x_{G\_Future,i,j} \tag{24}$$

where  $\overline{x_{obs,i}}$  and  $\overline{x_{G\_His,i}}$  are the average of observed and historical simulated streamflow in the  $i$ -th time period, and  $x_{G\_Future,i,j}$  is the future simulated streamflow in the  $i$ -th time period of the  $j$ -th year.

#### 4. Gravitational Search Algorithm

The gravitational search algorithm (GSA) is an evolutionary method based on Newton’s gravitational law [24]. In GSA, agents are considered as objects, and the gravitational forces among them will cause a global movement of all objects towards the objects with heavier masses, which represents an optimum solution in the search space. The position of agents which corresponds to a solution of the problem will be updated repeatedly until the termination condition is satisfied [43]. GSA has some advantages over PSO and central force optimization due to its good convergence and global search capabilities in dealing with benchmark functions [24]. Therefore, it has been widely used to solve reservoir optimization problems, such as multi-reservoir operation [44], operation of the Dez reservoir, a large-scale reservoir in Iran [45], and combined heat and power economic dispatch problems [46].

##### 4.1. Constraints Handling

Cascade reservoir operation is a highly-constrained problem. A set of water levels are chosen as agents, as shown in Equation (25):

$$X = \begin{bmatrix} X_1 \\ X_2 \\ \dots \\ X_N \end{bmatrix} = \begin{bmatrix} x_1^1, \dots, x_1^d, \dots, x_1^T \\ x_2^1, \dots, x_2^d, \dots, x_2^T \\ \dots \\ x_N^1, \dots, x_N^d, \dots, x_N^T \end{bmatrix} \tag{25}$$

where  $N$  is the number of reservoirs, and  $T$  is the number of time intervals.

Due to the complex constraints of reservoir operation problems, randomly-generated solutions are very unlikely to meet all constraints. As the initial population has an important effect on convergence speed, the feasibility of the solution in the initial population needs to be checked. If the solution is not feasible, a new feasible solution needs to be generated. In the random search stage, if the newly-generated solution fails to meet all the constraints, its feasible range should be adjusted using a two-way solution correction strategy. The feasible range of the water level  $x_{i+1}$  is defined as:

$$x_{i+1}^{max} = \min\left(x_i + \Delta z, Z\left(x_i, Q_i^{min}\right), Z\left(x_i, Q_i^{Pmin}\right), z^{max}\right) \tag{26}$$

$$x_{i+1}^{min} = \max\left(x_i - \Delta z, Z\left(x_i, Q_i^{max}\right), z^{min}\right) \tag{27}$$

$$Z(x_i, Q_i) = Z(V(x_i) + (I_i - Q_i)\Delta t) \tag{28}$$

where  $Q_i^{min}$  and  $Q_i^{max}$  are the minimum and maximum outflow of the reservoir, respectively.  $Q_i^{Pmin}$  is the minimum outflow for guaranteed output.  $z^{min}$  and  $z^{max}$  are the minimum and maximum water level, respectively.  $\Delta z$  is the limitation of the water level change.  $Z(V)$  and  $V(Z)$  are the relationship between water level and storage.

In the two-way solution correction strategy, the water level is adjusted at first to the feasible range from period 1 to  $T$ . If the correction fails at some unpredictable periods, then try to adjust the water level from period  $T$  to the breakpoint. If the correction still fails, the solution will be regarded as an infeasible solution.

#### 4.2. Implementation of GSA for LTHG

The long-term operation problem can be solved using GSA following the steps in Figure 6:

- Step 1 Randomly generate feasible initial solutions.
- Step 2 Evaluate the fitness of these solutions.
- Step 3 Update  $G(t)$ ,  $best(t)$ ,  $worst(t)$ , and  $M_i(t)$ .
- Step 4 Calculate the total force, acceleration, and velocity, and update the positions of the solutions.
- Step 5 Repeat Steps 2 to 5 until the termination criteria are met.

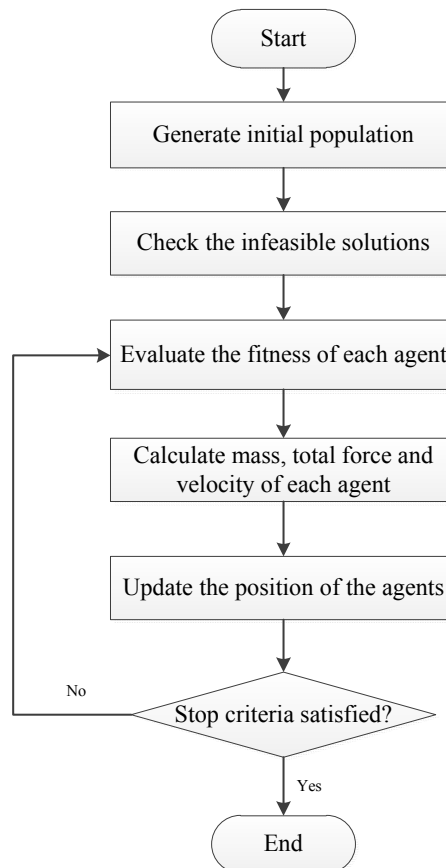


Figure 6. Flowchart of GSA.

## 5. Case Study

### 5.1. Historical Simulation of Hydropower Generation

In this section, the optimal scheduling scheme of the four cascade hydropower stations were obtained using the GSA algorithm, and compared with that obtained by the genetic algorithm (GA) and progressive optimality algorithm (POA). The parameter settings of GSA are  $G_0 = 100$ ,  $ms = 30$ ,  $w = 2$ ,  $c = 0.01$ , and the maximum evaluation time is set to 1000. The initial and end water levels of all reservoirs are set to the normal water level shown in Table 1. Each month is divided into three periods of approximately ten day each, resulting in 36 time intervals in a year. Streamflow data of three historical typical years including dry year (historical streamflow of 1977), normal year (1997), and wet year (1987) are chosen based on empirical distribution function of annual average streamflow. Each method is run 100 times, independently.

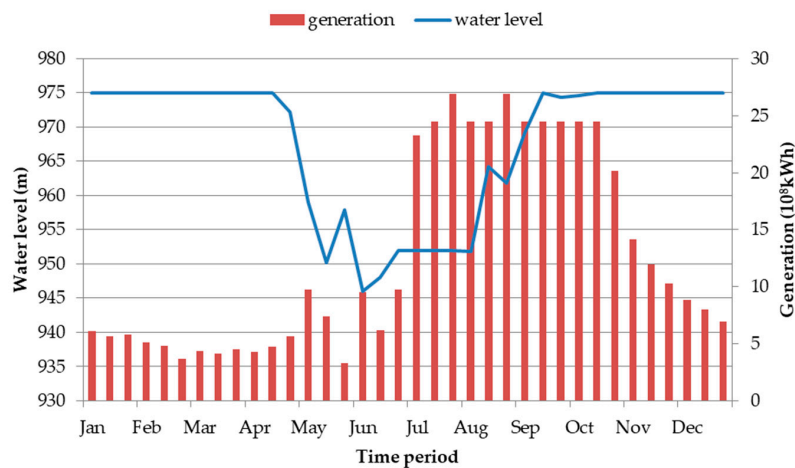
Table 5 shows the simulation results (mean, maximum and standard deviation of total power generation) obtained by GA, POA, and GSA. It clearly shows that GSA outperforms the

other two methods examined. The average power generation obtained by GSA is 201.9, 210.6, and 223.7 billion kWh in dry, normal, and wet years, with an increase of 10.0% and 0.7% in dry years, 9.7% and 0.6% in normal years, and 9.4% and 0.1% in wet years compared with that obtained by GA and POA, respectively.

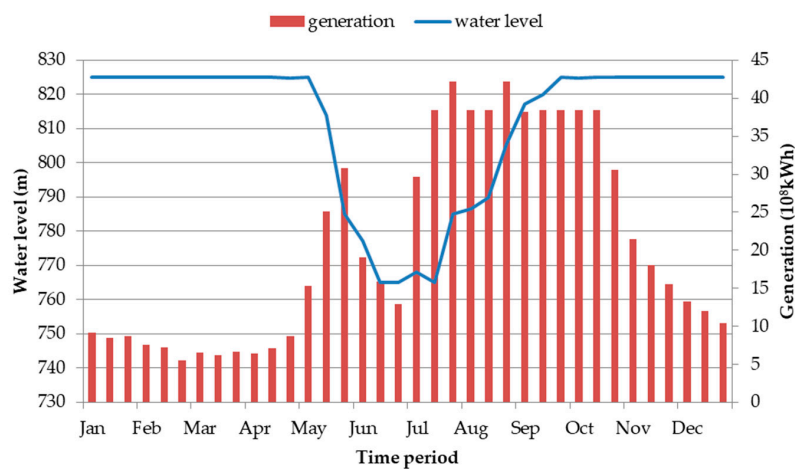
**Table 5.** Comparison of power generation ( $10^8$  kWh) among different methods.

Algorithm	Dry Year			Normal Year			Wet Year		
	Max.	Mean	Std.	Max.	Mean	Std.	Max.	Mean	Std.
GA	1875	1836	13.25	1964	1920	13.24	2095	2045	17.67
POA	2018	2006	25.18	2102	2094	7.72	2237	2234	2.92
GSA	2019	2019	0.03	2106	2106	0.37	2237	2237	0.05

Figure 7 shows the optimal results of the four hydropower stations in wet year as example. The water levels of the hydropower stations are kept at the normal water level from September to March, but drops below the flood limit water level in July and August. It shows that the fluctuation of the water level obtained by GSA is small. Thus indicating GSA can be used to solve the LTHG problem effectively.

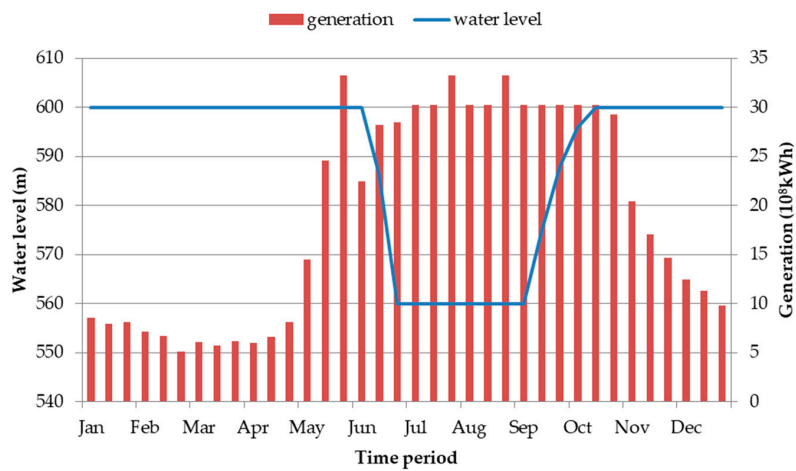


(a)

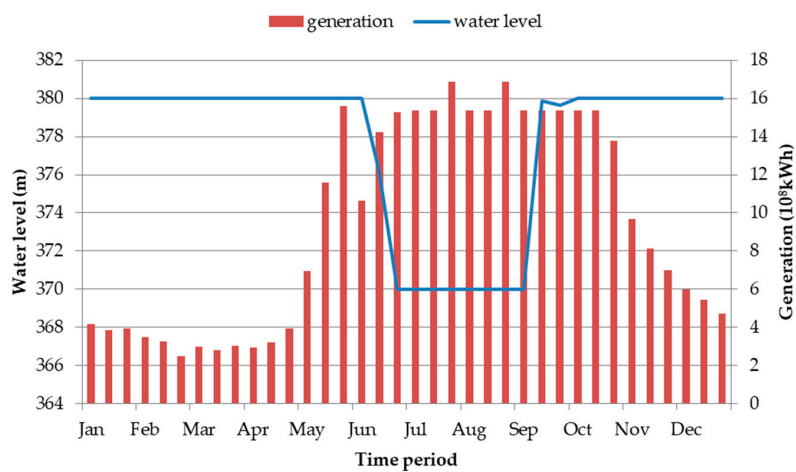


(b)

**Figure 7.** Cont.



(c)



(d)

**Figure 7.** The optimal results obtained by GSA in wet years: (a) Wudongde; (b) Baihetan; (c) Xiluodu; and (d) Xiangjiaba.

5.2. The Projection of Streamflow in the Context of Climate Change

In this section, we use the observed hydrological data before 1985 to calibrate the parameters of XAJ model. And the observed data from 1986 to 2000 was used to validate the performance of the model.

Figure 8 shows the simulated and observed daily streamflow of Pingshan station. Table 6 shows that both the linear regression correlation and Nash-Sutcliffe efficiency coefficient of Huatan and Pingshan stations are larger than 0.8. Therefore, the accuracy of the XAJ model was acceptable for daily streamflow projection.

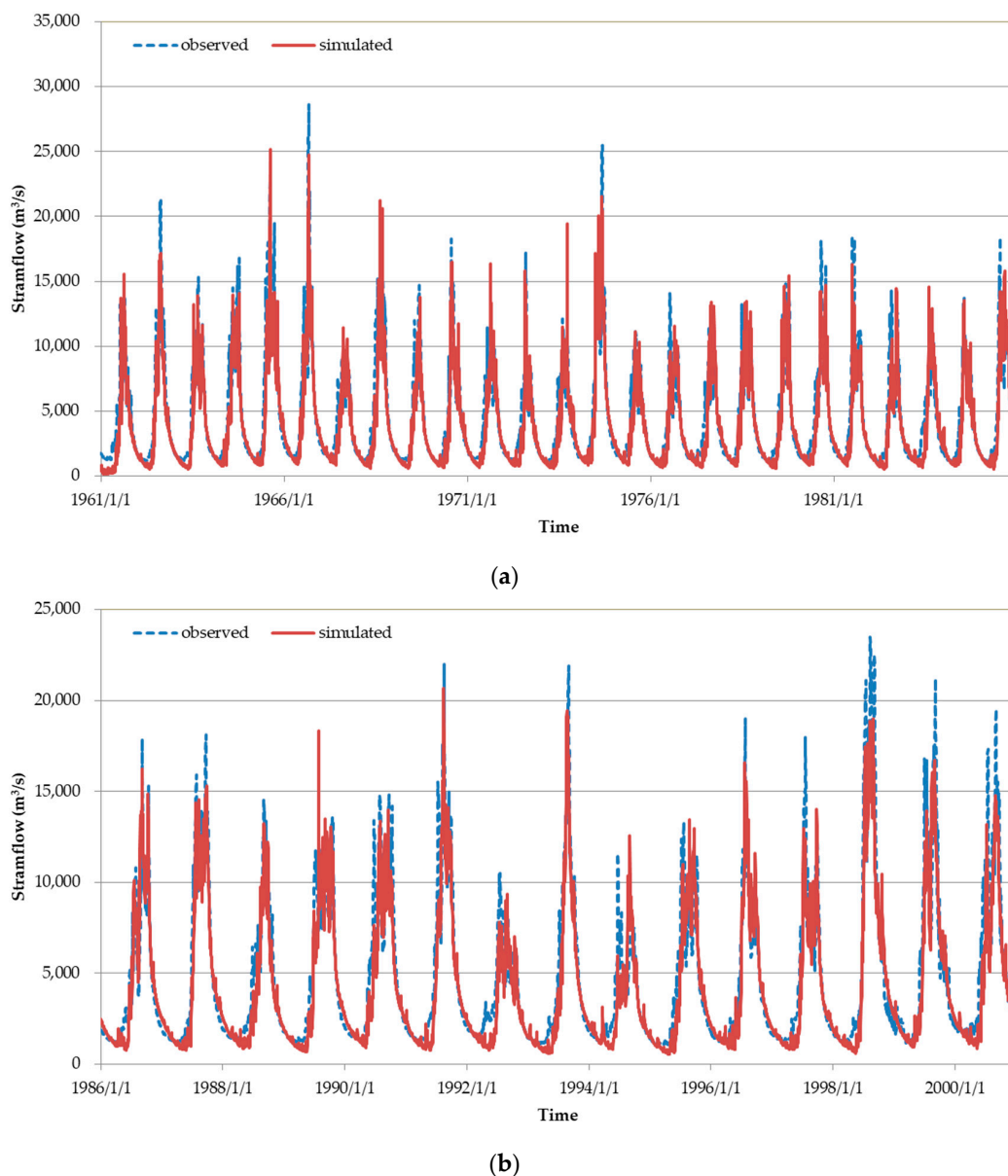


Figure 8. Simulated and observed daily streamflow of Pingshan station: (a) calibration, and (b) validation.

Table 6. Performance of XAJ model.

Station	Period	Time	Linear Regression Correlation	Nash-Sutcliffe Efficiency
Shigu	Calibration	1961–1985	0.767	0.752
	Validation	1986–2000	0.763	0.745
Panzhuhua	Calibration	1966–1985	0.847	0.840
	Validation	1986–2000	0.845	0.842
Huatan	Calibration	1977–1990	0.855	0.852
	Validation	1991–2000	0.868	0.848
Pingshan	Calibration	1961–1985	0.853	0.839
	Validation	1986–2000	0.854	0.842

In order to drive the LTHG model in Jinsha River, the streamflow of Huatan and Pingshan stations in the next 30 years (from 2021 to 2050) need to be projected. The precipitation and temperature data

from 1961 to 2050 given by five GCMs in three different scenarios was input to the parameterized XAJ model, and the daily streamflow in the context of climate change can be simulated. Mann-Kendall trend test [47] is used here to identify whether the data series shows increasing or decreasing trends:

$$sign(x_j - x_i) = \begin{cases} 1, & \text{if } x_j - x_i > 0 \\ 0, & \text{if } x_j - x_i = 0 \\ -1, & \text{if } x_j - x_i < 0 \end{cases} \quad (29)$$

$$S = \sum_{i=1}^{N-1} \sum_{j=i+1}^N sign(x_j - x_i) \quad (30)$$

$$VAR(S) = \frac{1}{18} \left[ n(n-1)(2n+5) - \sum_{p=1}^g t_p(t_p-1)(2t_p+5) \right] \quad (31)$$

$$Z = \begin{cases} \frac{S-1}{\sqrt{VAR(S)}}, & \text{if } S > 0 \\ 0, & \text{if } S = 0 \\ \frac{S+1}{\sqrt{VAR(S)}}, & \text{if } S < 0 \end{cases} \quad (32)$$

where  $n$  is the number of data series.  $g$  is the number of tied groups (a set a sample data having the same value).  $t_p$  is the number of data points in  $p$ th group. Defining the significance level as  $\alpha = 0.05$ , the data series has obvious trend if  $|Z| > 1.96$ .

The annual streamflow under different RCPs and GCMs is shown in Figure 9. Comparing with the annual streamflow in the baseline (from 1961 to 1990), it varies by 5.2%, 1.7%, and  $-0.3\%$  from 2021 to 2050 in RCP2.6, RCP4.5, and RCP8.5, respectively. The standard normal test statistic  $Z$  of RCP2.6, RCP4.5, and RCP8.5 during period 1961–2050 are 1.55, 0.37, and  $-0.52$ , respectively. It shows an increasing trend during 1961–2050 in RCP2.6 and RCP4.5, while a decreasing trend during 1961–2050 is reflected in RCP8.5. However, all the  $|Z|$  values are smaller than 1.96, indicating that the trends are not significant. According to the empirical distribution function of annual average streamflow of Pingshan station, we selected the typical year in 2021 to 2050. The annual streamflow in wet, normal, and dry years under different scenarios are shown in Table 7.

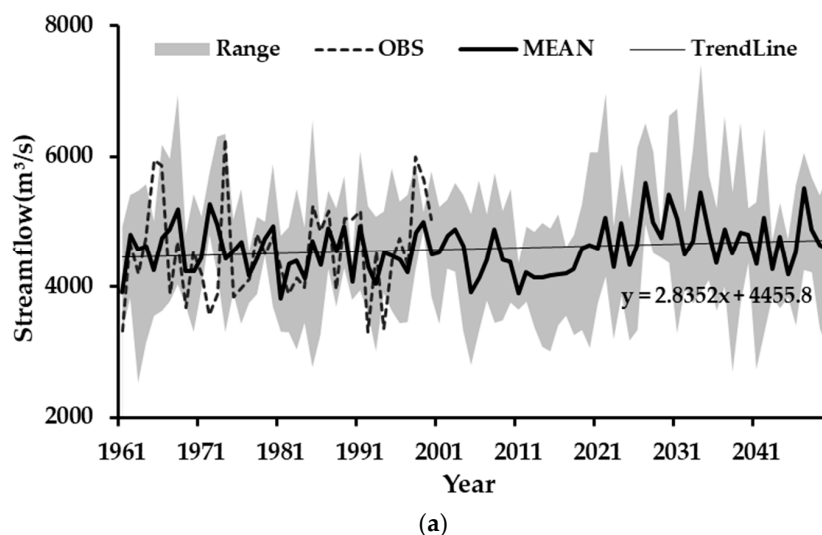


Figure 9. Cont.

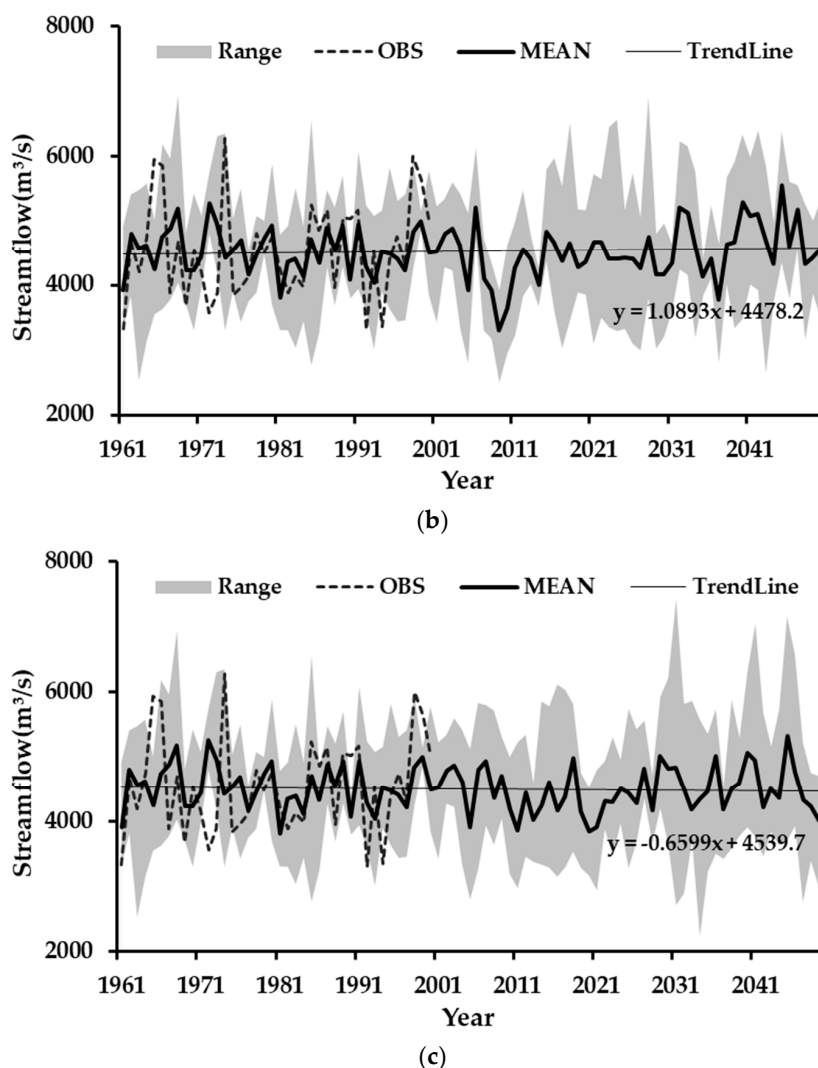


Figure 9. Annual streamflow in Pingshan Station under different scenarios: (a) RCP2.6, (b) RCP4.5, and (c) RCP8.5.

Table 7. Annual streamflow (m<sup>3</sup>/s) of Pingshan station in typical years.

GCM	Dry Year (75%) m <sup>3</sup> /s (Year)	Normal Year (50%) m <sup>3</sup> /s (Year)	Wet Year (25%) m <sup>3</sup> /s (Year)
RCP2.6_GFDL-ESM2M	4202 (2037) *	4857 (2029)	5569 (2047)
RCP2.6_HADGEM2-ES	3931 (2026)	4368 (2030)	5020 (2048)
RCP2.6_IPSL-CM5A-LR	4083 (2045)	4769 (2029)	5500 (2037)
RCP2.6_MIROC-ESM-CHEM	4292 (2048)	4720 (2028)	5448 (2034)
RCP2.6_NORESM1-M	4513 (2025)	4762 (2023)	5090 (2035)
RCP4.5_GFDL-ESM2M	3484 (2050)	4456 (2027)	5052 (2042)
RCP4.5_HADGEM2-ES	4000 (2023)	4359 (2038)	4644 (2037)
RCP4.5_IPSL-CM5A-LR	4293 (2029)	4756 (2022)	5448 (2021)
RCP4.5_MIROC-ESM-CHEM	3703 (2030)	4648 (2031)	5262 (2048)
RCP4.5_NORESM1-M	4278 (2044)	4647 (2040)	5312 (2047)
RCP8.5_GFDL-ESM2M	3886 (2033)	4343 (2022)	4789 (2021)
RCP8.5_HADGEM2-ES	4029 (2047)	4421 (2040)	4595 (2045)
RCP8.5_IPSL-CM5A-LR	3737 (2033)	4436 (2034)	5316 (2027)
RCP8.5_MIROC-ESM-CHEM	4208 (2029)	4626 (2038)	5683 (2042)
RCP8.5_NORESM1-M	3824 (2041)	4099 (2023)	4968 (2047)

Note: \* PS: The number in the bracket represent the typical year.

5.3. Impact of Future Climate Changes on Reservoir Scheduling

In this section, we discuss the impact of future climate changes on the total hydropower generation of the cascade reservoirs in Jinsha River. Figure 10 shows the mean, maximum, and minimum total power generation change of the five GCMs under three different climate change scenarios.

In RCP2.6, the average changes in dry, normal, and wet years are 4.7%, 2.5%, and 1.8%, respectively, which shows an increase in three typical years. Among the 15 combinations (five GCMs under three scenarios), 80% are positive and 20% are negative, showing good consistency. In RCP8.5, the average changes of the five GCMs on three typical years are -1.4%, -2.3%, and -1.2%, respectively, which shows a decrease in three typical years. However, 66% of the 15 combinations are positive, while 33% of them are negative, showing poor consistency. In RCP4.5, there are large differences among the five GCMs, resulting in an average value of the GCMs around 0.

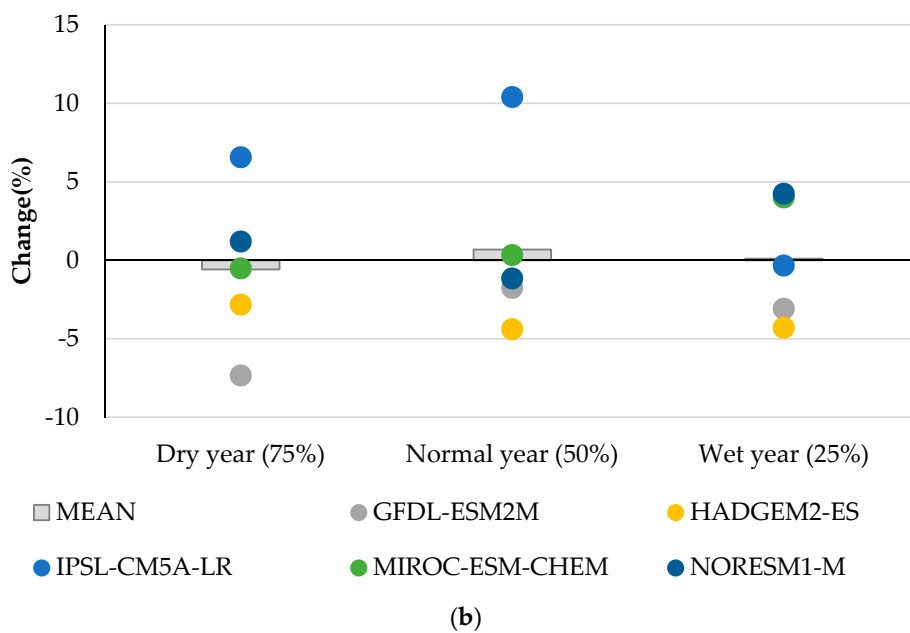
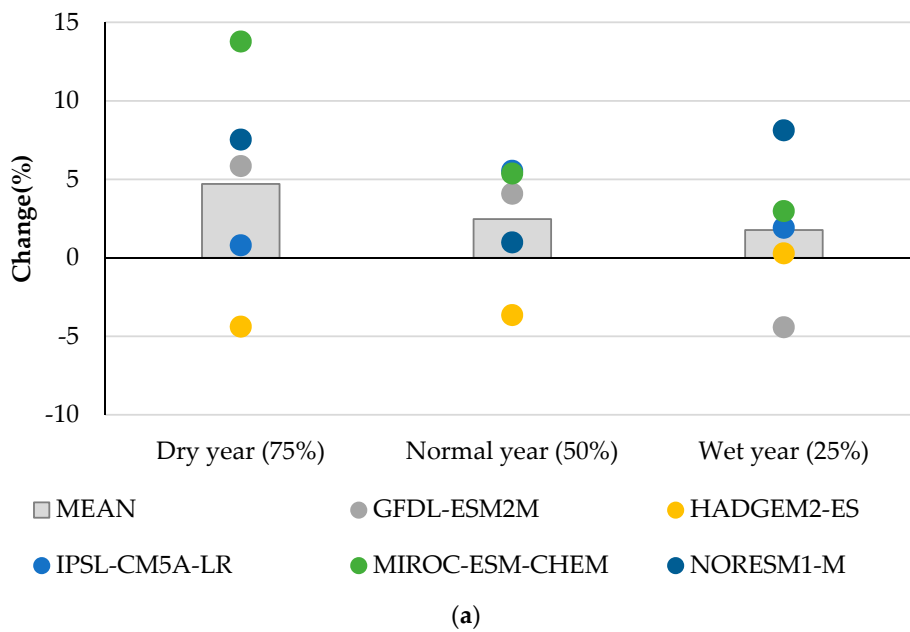


Figure 10. Cont.

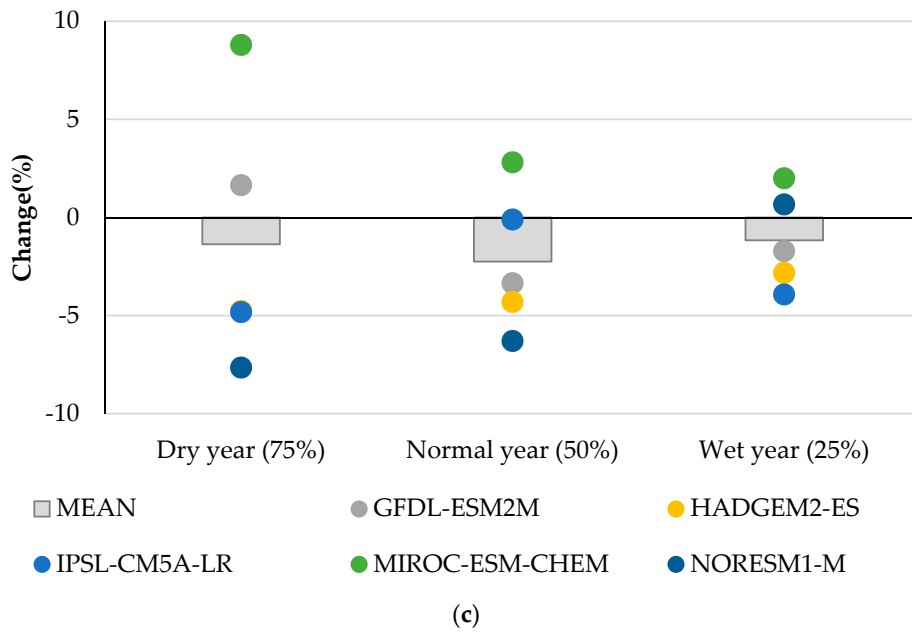


Figure 10. Power generation change under scenario (a) RCP2.6; (b) RCP4.5; and (c) RCP8.5.

Figure 11 shows the power generation in the next 30 years and in historical average under three different climate change scenarios. Figure 11a shows the results under scenario RCP2.6. The average power generations in next three decades are all larger than the historical average power generation, indicating that the power generation in the future will increase. The generation results of the five GCMs are similar and the uncertainty range are (−4.3%, 4.0%), (−5.2%, 3.9%) and (−4.2%, 5.4%). As shown in Figure 11b, the average power generation changes in the next three decades under scenario RCP4.5 are −3.8%, 0.4%, and 1.9%, respectively. However, the results of the five GCMs show a large range in 2021–2030 and 2041–2050. The uncertainty range in the next three decades are (−12.4%, 10.0%), (−4.7%, 3.8%), and (−9.1%, 8.0%), showing a great deal of uncertainty. In Figure 11c, the average power generation under RCP8.5 will decrease in 2021–2030 and increase in 2031–2040. The uncertainty range in 2031–2040 and 2041–2050 show a large divergence in the five GCMs.

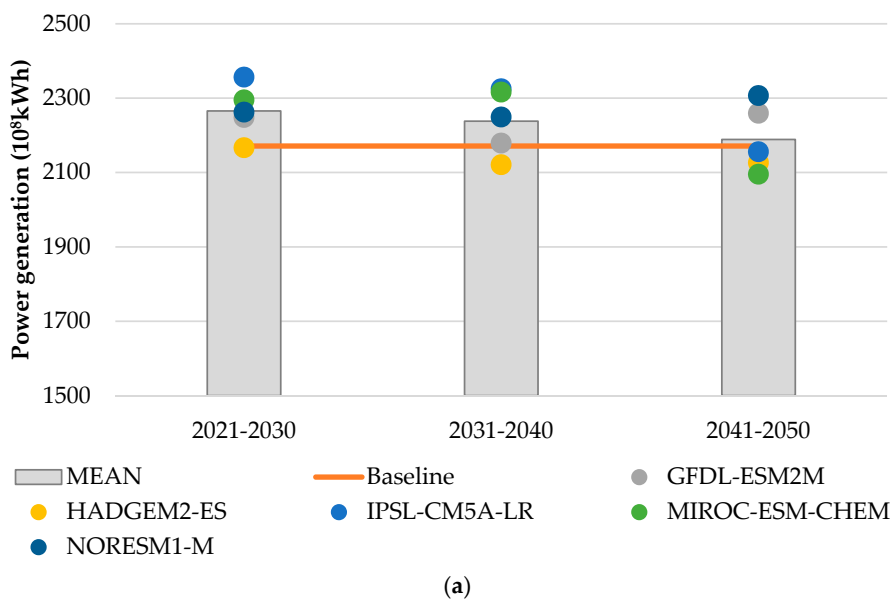
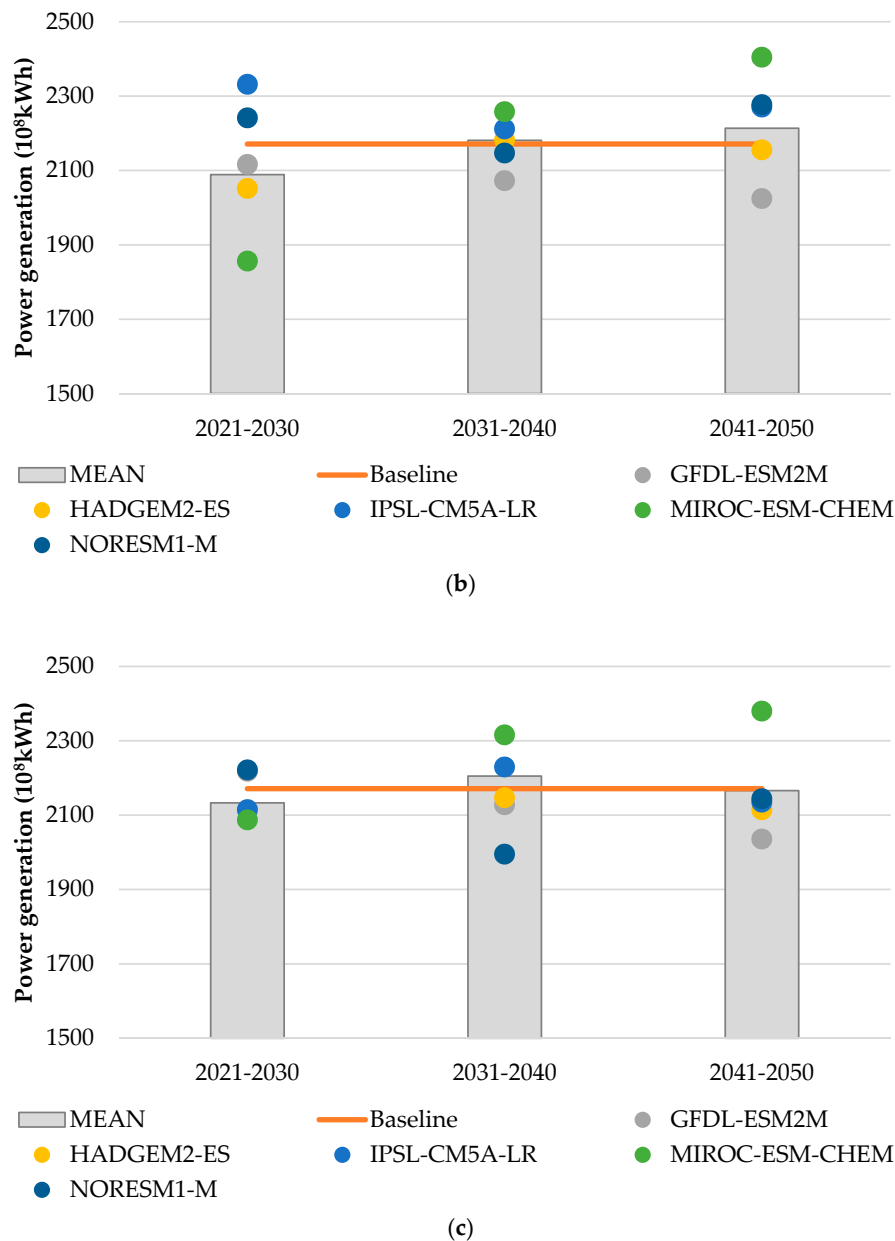


Figure 11. Cont.



**Figure 11.** Power generation in the next three decades under scenario (a) RCP2.6; (b) RCP4.5; and (c) RCP8.5.

### 6. Conclusions

In this paper, we evaluate the impacts of future climate changes on LTHG in the Jinsha River. The streamflow in the future is projected based on five GCMs, and three climate change scenarios are considered. The XAJ model was used to simulate daily streamflow, and then GSA was adopted to solve the LTHG problems.

In case studies, the comparison among three algorithms shows that GSA can be used to solve LTHG problem effectively in Jinsha River. Validation of the XAJ model shows that it is suitable for streamflow projection in Jinsha River, with the linear regression correlation and Nash-Sutcliffe efficiency are high than 0.7. Comparing with the historical average annual streamflow, that average annual streamflow from 2021 to 2050 varies 5.2%, 1.7%, and  $-0.3\%$  in RCP2.6, RCP4.5, and RCP8.5, respectively. The standard normal test statistic  $Z$  shows an increasing trend during the period 1961–2050

in RCP2.6 and RCP4.5, while a decreasing trend occurring during the period 1961–2050 is reflected in RCP8.5. However, all these trends are not significant.

Future climate changes are expected to have an impact on reservoir inflow in the downstream of the Jinsha River. Simulation results on typical years show that the different climate change scenarios have different impacts on hydropower generation. In RCP2.6, the average changes in dry, normal, and wet years are 4.7%, 2.5%, and 1.8%. In RCP8.5 the average changes are −1.4%, −2.3%, and −1.2%, respectively. In RCP4.5, the results of the five GCMs vary widely. After simulating the power generation in next 30 years, we found that average power generations in the next three decades will increase under scenario RCP2.6. However, results under RCP4.5 and RCP8.5 show a large uncertainty range, the five GCMs have a large divergence on the three climate change scenarios.

Overall, the impacts of future climate changes on hydropower generation need to be taken into consideration for plan-making. The above results will help us adapt hydropower station operational plans to counteract the effects of climate change. However, other uncertainties, such as the hydrological model, have not been discussed in this paper. Additionally, studies have shown that the original GSA has drawbacks, such as weak local exploitation capability and slow convergence rate in its final iterations. Further research is underway to include more GCMs and perform uncertainty analyses. The optimal method for LTHG also needs to be improved, and the scheduling model needs to be extended to deal with risk analysis on reservoir scheduling.

**Acknowledgments:** This work is supported by the National Key R and D Program of China (2016YFC0402205), the Key Program of the Major Research Plan of the National Natural Science Foundation of China (No. 91547208), the National Natural Science Foundation of China (No. 51479075, No. 51409008), and the National Public Research Institutes for Basic R and D Operating Expenses Special Project (No. CKSF2017008/SZ). We also acknowledge the entire development team, without whose help this research could not have been achieved.

**Author Contributions:** Yu Feng and Chao Wang conceived and designed the study. Yu Feng and Chao Wang wrote the GSA algorithm. Li Mo performed the comparison between different methods. Zhe Yuan and Jiang Wu wrote the forecast model and performed the future streamflow simulation. Peilun Zhang and Yongqiang Wang performed the historical scheduling simulation. Final checks were done by Jianzhong Zhou. All authors have read and approved the final manuscript.

**Conflicts of Interest:** The authors declare no conflict of interest.

## References

1. Zhao, T.; Zhao, J.; Liu, P.; Lei, X. Evaluating the marginal utility principle for long-term hydropower scheduling. *Energy Convers. Manag.* **2015**, *106*, 213–223. [[CrossRef](#)]
2. Liu, Y.; Sang, Y.F.; Li, X.; Hu, J.; Liang, K. Long-Term Streamflow Forecasting Based on Relevance Vector Machine Model. *Water* **2016**, *9*. [[CrossRef](#)]
3. Xu, W.; Zhang, C.; Peng, Y.; Fu, G.; Zhou, H. A two stage Bayesian stochastic optimization model for cascaded hydropower systems considering varying uncertainty of flow forecasts. *Water Resour. Res.* **2014**, *50*, 9267–9286. [[CrossRef](#)]
4. Zambelli, M.S.; Luna, I.; Soares, S. Long-term hydropower scheduling based on deterministic nonlinear optimization and annual inflow forecasting models. In Proceedings of the 2009 IEEE PowerTech, Bucharest, Romania, 28 June–2 July 2009; pp. 1–8.
5. Lohmann, T.; Hering, A.S.; Rebennack, S. Spatio-temporal hydro forecasting of multireservoir inflows for hydro-thermal scheduling. *Eur. J. Oper. Res.* **2016**, *255*, 243–258. [[CrossRef](#)]
6. Intergovernmental Panel on Climate Change. *Climate Change 2013: The Physical Science Basis*; Cambridge University Press: Cambridge, UK, 2013; Volume 43, pp. 866–871.
7. Haddeland, I.; Heinke, J.; Biemans, H.; Eisner, S.; Flörke, M.; Hanasaki, N.; Konzmann, M.; Ludwig, F.; Masaki, Y.; Schewe, J. Global water resources affected by human interventions and climate change. *Proc. Natl. Acad. Sci. USA* **2014**, *111*, 3251–3256. [[CrossRef](#)] [[PubMed](#)]
8. Gaudard, L.; Romerio, F.; Dalla Valle, F.; Gorret, R.; Maran, S.; Ravazzani, G.; Stoffel, M.; Volonterio, M. Climate change impacts on hydropower in the Swiss and Italian Alps. *Sci. Total Environ.* **2014**, *493*, 1211–1221. [[CrossRef](#)] [[PubMed](#)]

9. Pereira-Cardenal, S.J.; Madsen, H.; Arnbjerg-Nielsen, K.; Riegels, N.; Jensen, R.; Mo, B.; Wangenstein, I.; Bauer-Gottwein, P. Assessing climate change impacts on the Iberian power system using a coupled water-power model. *Clim. Chang.* **2014**, *126*, 351–364. [[CrossRef](#)]
10. Turner, S.W.D.; Hejazi, M.; Kim, S.H.; Clarke, L.; Edmonds, J. Climate impacts on hydropower and consequences for global electricity supply investment needs. *Energy* **2017**, *141*, 2081–2090. [[CrossRef](#)]
11. Taylor, K.E.; Stouffer, R.J.; Meehl, G.A. An Overview of CMIP5 and the Experiment Design. *Bull. Am. Meteorol. Soc.* **2012**, *93*, 485–498. [[CrossRef](#)]
12. Moss, R.H.; Edmonds, J.A.; Hibbard, K.A.; Manning, M.R.; Rose, S.K.; Vuuren, D.P.V.; Carter, T.R.; Emori, S.; Kainuma, M.; Kram, T. The next generation of scenarios for climate change research and assessment. *Nature* **2010**, *463*. [[CrossRef](#)] [[PubMed](#)]
13. Liao, X.; Zhou, J.; Ouyang, S.; Zhang, R.; Zhang, Y. An adaptive chaotic artificial bee colony algorithm for short-term hydrothermal generation scheduling. *Int. J. Electr. Power Energy Syst.* **2013**, *53*, 34–42. [[CrossRef](#)]
14. Tian, H.; Yuan, X.; Ji, B.; Chen, Z. Multi-objective optimization of short-term hydrothermal scheduling using non-dominated sorting gravitational search algorithm with chaotic mutation. *Energy Convers. Manag.* **2014**, *81*, 504–519. [[CrossRef](#)]
15. Liao, X.; Zhou, J.; Zhang, R.; Zhang, Y. An adaptive artificial bee colony algorithm for long-term economic dispatch in cascaded hydropower systems. *Int. J. Electr. Power Energy Syst.* **2012**, *43*, 1340–1345. [[CrossRef](#)]
16. Wang, C.; Zhou, J.; Peng, L.; Liu, Y. Long-term scheduling of large cascade hydropower stations in Jinsha River, China. *Energy Convers. Manag.* **2015**, *90*, 476–487. [[CrossRef](#)]
17. Zhang, H.; Zhou, J.; Fang, N.; Zhang, R.; Zhang, Y. An efficient multi-objective adaptive differential evolution with chaotic neuron network and its application on long-term hydropower operation with considering ecological environment problem. *Int. J. Electr. Power Energy Syst.* **2013**, *45*, 60–70. [[CrossRef](#)]
18. Soares, S.; Ohishi, T.; Cicogna, M.; Arce, A. Dynamic dispatch of hydro generating units. In Proceedings of the 2003 IEEE Power Tech Conference Proceedings, Bologna, Italy, 23–26 June 2003; Volume 2, p. 6.
19. Cheng, C.T.; Liao, S.L.; Tang, Z.T.; Zhao, M.Y. Comparison of particle swarm optimization and dynamic programming for large scale hydro unit load dispatch. *Energy Convers. Manag.* **2009**, *50*, 3007–3014. [[CrossRef](#)]
20. Nanda, J.; Bijwe, P.R. Optimal Hydrothermal Scheduling with Cascaded Plants Using Progressive Optimality Algorithm. *IEEE Trans. Power App. Syst.* **1981**, *PAS-100*, 2093–2099. [[CrossRef](#)]
21. Cheng, C.; Shen, J.; Wu, X. Short-Term Scheduling for Large-Scale Cascaded Hydropower Systems with Multivibration Zones of High Head. *J. Water Resour. Plan. Manag.* **2011**, *138*, 257–267. [[CrossRef](#)]
22. Chang, H.-H. Genetic algorithms and non-intrusive energy management system based economic dispatch for cogeneration units. *Energy* **2011**, *36*, 181–190. [[CrossRef](#)]
23. Wang, J.; Huang, W.; Ma, G.; Chen, S. An improved partheno genetic algorithm for multi-objective economic dispatch in cascaded hydropower systems. *Int. J. Electr. Power Energy Syst.* **2015**, *67*, 591–597. [[CrossRef](#)]
24. Rashedi, E.; Nezamabadi-Pour, H.; Saryazdi, S. GSA: A Gravitational Search Algorithm. *Intell. Inf. Manag.* **2012**, *4*, 390–395. [[CrossRef](#)]
25. Xu, Y.; Zhou, J.; Xue, X.; Fu, W.; Zhu, W.; Li, C. An adaptively fast fuzzy fractional order PID control for pumped storage hydro unit using improved gravitational search algorithm. *Energy Convers. Manag.* **2016**, *111*, 67–78. [[CrossRef](#)]
26. Zhao, R.J. The Xinanjiang model applied in China. *J. Hydrol.* **1992**, *135*, 371–381.
27. Lü, H.; Hou, T.; Horton, R.; Zhu, Y.; Chen, X.; Jia, Y.; Wang, W.; Fu, X. The streamflow estimation using the Xinanjiang rainfall runoff model and dual state-parameter estimation method. *J. Hydrol.* **2013**, *480*, 102–114. [[CrossRef](#)]
28. Nash, J.E.; Sutcliffe, J.V. River flow forecasting through conceptual models part I—A discussion of principles. *J. Hydrol.* **1970**, *10*, 282–290. [[CrossRef](#)]
29. Jie, C.; Brissette, F.P.; Annie, P.; Robert, L. Overall uncertainty study of the hydrological impacts of climate change for a Canadian watershed. *Water Resour. Res.* **2011**, *47*, 1–16.
30. Kay, A.L.; Davies, H.N.; Bell, V.A.; Jones, R.G. Comparison of uncertainty sources for climate change impacts: Flood frequency in England. *Clim. Chang.* **2009**, *92*, 41–63. [[CrossRef](#)]
31. Wu, C.H.; Huang, G.R.; Yu, H.J. Prediction of extreme floods based on CMIP5 climate models: A case study in the Beijiang River basin, South China. *Hydrol. Earth Syst. Sci.* **2015**, *11*, 1385–1399. [[CrossRef](#)]

32. Scarcelli, R.O.C.; Zambelli, M.S.; Soares, S.; Carneiro, A.A.F.M. Ensemble of Markovian stochastic dynamic programming models in different time scales for long term hydropower scheduling. *Electr. Power Syst. Res.* **2017**, *150*, 129–136. [[CrossRef](#)]
33. Tarroja, B.; Aghakouchak, A.; Samuelson, S. Quantifying climate change impacts on hydropower generation and implications on electric grid greenhouse gas emissions and operation. *Energy* **2016**, *111*, 295–305. [[CrossRef](#)]
34. Warszawski, L.; Frieler, K.; Huber, V.; Piontek, F.; Serdeczny, O.; Schewe, J. The Inter-Sectoral Impact Model Intercomparison Project (ISI-MIP): Project framework. *Proc. Natl. Acad. Sci. USA* **2014**, *111*, 3228–3232. [[CrossRef](#)] [[PubMed](#)]
35. Hempel, S.; Frieler, K.; Warszawski, L.; Schewe, J.; Piontek, F. A trend-preserving bias correction—The ISI-MIP approach. *Earth Syst. Dyn.* **2013**, *4*, 219–236. [[CrossRef](#)]
36. Yuan, F.; Tung, Y.K.; Ren, L. Projection of future streamflow changes of the Pearl River basin in China using two delta-change methods. *Hydrol. Res.* **2016**, *47*, 217–238. [[CrossRef](#)]
37. Wang, J.; Shi, P.; Jiang, P.; Hu, J.; Qu, S.; Chen, X.; Chen, Y.; Dai, Y.; Xiao, Z. Application of BP Neural Network Algorithm in Traditional Hydrological Model for Flood Forecasting. *Water* **2017**, *9*, 48. [[CrossRef](#)]
38. Chen, J.; Yang, X. Optimal parameter estimation for Muskingum model based on Gray-encoded accelerating genetic algorithm. *Commun. Nonlinear Sci. Numer. Simul.* **2007**, *12*, 849–858. [[CrossRef](#)]
39. Berti, A.; Tardivo, G.; Chiaudani, A.; Rech, F.; Borin, M. Assessing reference evapotranspiration by the Hargreaves method in north-eastern Italy. *Agric. Water Manag.* **2014**, *140*, 20–25. [[CrossRef](#)]
40. Wang, W.C.; Cheng, C.T.; Chau, K.W.; Xu, D.M. Calibration of Xinanjiang model parameters using hybrid genetic algorithm based fuzzy optimal model. *J. Hydroinform.* **2012**, *14*, 784–799. [[CrossRef](#)]
41. Moriasi, D.N.; Arnold, J.G.; Van Liew, M.W.; Bingner, R.L.; Harmel, R.D.; Veith, T.L. Model evaluation guidelines for systematic quantification of accuracy in watershed simulations. *Trans. Asabe* **2007**, *50*, 885–900. [[CrossRef](#)]
42. Yuan, Z.; Yang, Z.; Yan, D.; Yin, J. Historical changes and future projection of extreme precipitation in China. *Theor. Appl. Climatol.* **2017**, *127*, 393–407. [[CrossRef](#)]
43. Mishra, A.; Kumar, G.V.N. Congestion Management of Deregulated Power Systems by Optimal Setting of Interline Power Flow Controller using Gravitational Search Algorithm. *J. Electr. Syst. Inf. Technol.* **2016**, *4*, 198–212. [[CrossRef](#)]
44. Bozorg-Haddad, O.; Janbaz, M.; Loáiciga, H.A. Application of the gravity search algorithm to multi-reservoir operation optimization. *Adv. Water Resour.* **2016**, *98*, 173–185. [[CrossRef](#)]
45. Moeini, R.; Soltani-Nezhad, M.; Daei, M. Constrained gravitational search algorithm for large scale reservoir operation optimization problem. *Eng. Appl. Artif. Intell.* **2017**, *62*, 222–233. [[CrossRef](#)]
46. Beigvand, S.D.; Abdi, H.; Scala, M.L. Combined heat and power economic dispatch problem using gravitational search algorithm. *Electr. Power Syst. Res.* **2016**, *133*, 160–172. [[CrossRef](#)]
47. Gocic, M.; Trajkovic, S. Analysis of changes in meteorological variables using Mann-Kendall and Sen's slope estimator statistical tests in Serbia. *Glob. Planet. Chang.* **2013**, *100*, 172–182. [[CrossRef](#)]

